Ingeniería y Competitividad
Vol 28 (1) 2026 doi: 10.25100/iyc.v28i1.15228

Vol 28 (1)

ISSN
0123-3033
e- 2027-8284

Original Article

Multitask Convolutional Neural Network for Spatiotemporal Precipitation Estimation in Andean Regions

Red Neuronal Convolucional Multitarea para la Estimación Espaciotemporal de Precipitaciones en Regiones Andinas

Henry Rubiano[1] Miguel Barrios[1] Cristian Guevara[1]

[1]Computational Hydrology and Hydraulics Lab, Universidad del Tolima, Ibagué, Colombia.

Abstract

Introduction: The Colombian Andes present limitations for spatial estimation of precipitation due to scarce rainfall instrumentation and high variability influenced by phenomena such as El Niño. Therefore, it is necessary to develop approaches to merge remote sensing data with terrestrial observations and improve the spatiotemporal modeling of precipitation.
Objectives: To implement a multitask convolutional neural network model with U-Net architecture to estimate rainfall probability (classification) and precipitation rate (regression), with a resolution of 2 km and 10 minutes in an Andean region of Colombia.
Metodology: The study was conducted in the Colombian Andean zone, using pluviometric data, meteorological radar, and GOES-16 satellite. A convolutional neural network with U-Net architecture was implemented to estimate precipitations, with data distributed in proportions of 70%, 15%, and 15% for training, validation, and testing. The model evaluation was carried out with classification and regression metrics.
Results: The model shows satisfactory efficiency for detecting rainfall events, with an area under the ROC curve close to 0.8, demonstrating a high capacity to classify the spatial pattern of its occurrence. In contrast, the convolutional network has lower performance in the task of quantifying rainfall millimeters, with Pearson correlation values on the order of 0.6 in training and validation.
Conclusions: The use of convolutional neural networks achieves satisfactory classifications of rainfall events; however, it tends to underestimate the precipitation rate under conditions of scarce information.

Keywords: convolutional neural networks; precipitation; mathematical modeling; satellite; radar.

Resumen

Introducción: los andes colombianos presentan limitaciones para la estimación espacial de la precipitación, debido a la escasa instrumentación pluviométrica y la alta variabilidad influida por fenómenos como El Niño. Por ello se hace necesario desarrollar enfoques para fusionar datos de teledetección con observaciones terrestres y mejorar la modelación espaciotemporal de la lluvia.
Objetivos: Implementar un modelo de red neuronal convolucional multitarea con arquitectura U-Net para estimar simultáneamente la probabilidad de lluvia (clasificación) y la tasa de precipitación (regresión), con resolución de 2 km y 10 minutos en una región andina.
Metodología: El estudio se realizó en la zona andina colombiana, usando datos pluviométricos, radar meteorológico, y satélite GOES-16. Se implementó una red neuronal convolucional con arquitectura U-Net para estimar precipitaciones, con datos distribuidos en proporciones de 70%, 15%, y 15% para entrenamiento, validación y prueba, la evaluación del modelo se llevó a cabo con métricas de clasificación y regresión.
Resultados: El modelo presenta una eficiencia satisfactoria para la detección de eventos de lluvia, con un área bajo la curva ROC cercana a 0.8, demostrando una alta capacidad para clasificar el patrón espacial de su ocurrencia. En contraste, la red convolucional tiene un inferior desempeño en la tarea de cuantificación de los milímetros de lluvia, con valores de correlación de Pearson del orden de 0.6 en entrenamiento y validación.
Conclusiones: El uso de redes neuronales convolucionales logra clasificaciones satisfactorias de los eventos de lluvia, sin embargo tiende a subestimar la tasa de precipitación en condiciones de información escasa.

Palabras clave: redes neuronal convolucionales; precipitación; modelación matemática; satélite; radar.

How to cite?

Rubiano H, Barrios M, Guevara C. Multitask Convolutional Neural Network for Spatiotemporal Precipitation Estimation in Andean Regions. Ingeniería y Competitividad, 2026, 28(1) e-20515228

https://doi.org/10.25100/iyc.v28i1.15228

Received: 12/09/25
Reviewed: 20/10/25
Accepted: 21/01/26
Online: 18/02/26

Correspondence

hgrubianos@ut.edu.co

Spanish version

Why was it done?
The study was conducted to overcome the limitations of sparse pluviometry instrumentation in the Colombian Andes, where low station density and high orographic/ENSO-driven variability hinder accurate spatial precipitation estimation. It aimed to leverage remote sensing data (GOES-16 satellite and radar) fused with point observations through deep learning, generating sub-hourly reconstructions (2 km / 10 min) useful for hydrological modeling, extreme event forecasting, and water resource management in vulnerable areas with limited meteorological infrastructure.

What were the most relevant results?
The model achieved satisfactory performance in the classification task (rain/no-rain detection), reaching AUC ≈ 0.80, POD of 0.80–0.85, and FAR ≈ 0.21 in validation and test sets. In contrast, quantitative precipitation estimation was markedly weaker, with RMSE ≈ 1.02–1.07 mm/10 min, MAE ≈ 0.44–0.51 mm, and very low R^2 (0.05–0.36), showing systematic underestimation of intense events and high scatter, revealing the difficulties of a pure CNN architecture in capturing temporal dependencies and extreme magnitudes.

What do they contribute?
The study demonstrates that a multitask U-Net can adequately detect the spatial occurrence of rainfall even with very few rain gauges, providing a useful binary product for nowcasting and early warning in the Andes. At the same time, it clearly exposes the current limitations of CNNs in accurate sub-hourly quantitative precipitation estimation in data-scarce environments, reinforcing the need for hybrid architectures and increased gauge density to improve regression performance. It offers a realistic, diagnostic benchmark valuable for future developments in similar tropical mountainous regions.

Graphical Abstract

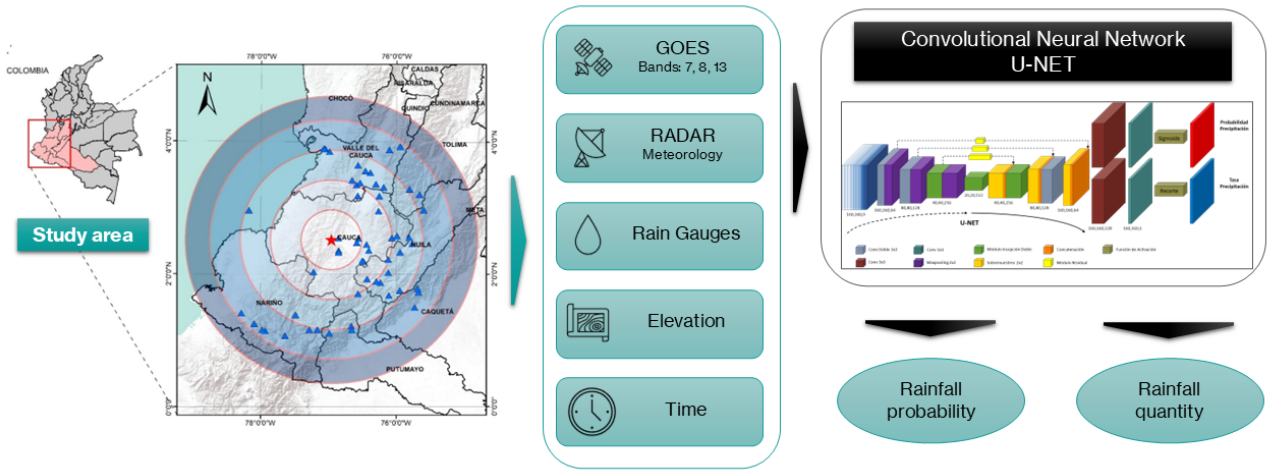

doi: 10.25100/iyc.v28i1.15228

Introduction

Understanding the spatiotemporal variability of precipitation is fundamental for developing modeling tools and water resource management strategies that support decision-making for its sustainable use and exploitation. However, spatiotemporal rainfall estimation in the Andean context is limited by the insufficient availability of rain gauge stations (1). This scarcity of data is particularly critical in hydroclimatic studies, especially in developing countries facing high costs associated with establishing and maintaining meteorological infrastructure (2,3). n this context, the need to generate alternatives to address the limited availability of pluviometry information has increased due to advances in the implementation of machine learning algorithms and the growing availability of remote sensing products for meteorological monitoring (4).

In recent years, various machine learning algorithms have been applied to estimate precipitation by merging satellite-based products with rain gauge observations. Chen et al. (5) proposed a machine learning approach to generate high-resolution (1 km) daily precipitation estimates by combining satellite data and ground observations. Similarly, Zhang et al. (6) presented a double machine learning approach to merge multiple satellite-based precipitation products with rain gauge observations, achieving significant bias reduction. These approaches have successfully captured complex nonlinear patterns for precipitation estimation; however, machine learning tools have been scarcely applied to high-temporal-resolution (10-minute) precipitation modeling in areas with sparse instrumentation, such as the Andean region.

Within the field of Machine Learning, Deep Learning techniques have gained relevance due to their ability to recognize nonlinear patterns and complex features in large datasets. Convolutional Neural Networks (CNNs) are particularly effective in tasks such as image classification, object recognition, and spatiotemporal sequence processing, including weather prediction (7). In the context of precipitation, CNNs have been used to process and analyze satellite and radar images, as well as other spatial data, identifying complex patterns correlated with rainfall events, such as certain cloud formations, low-pressure systems, or storm fronts (8–11).

The objective of this study is to evaluate the capability of CNNs in reconstructing historical sub-hourly precipitation time series (10-minute intervals) and reproducing the spatial pattern of rainfall occurrence at 2 km resolution, using a multitask network trained on observed ground-based meteorological information and remote sensors (satellite and radar), in a context of scarce pluviometry information. Through this research, knowledge is contributed regarding rainfall behavior and variability to support climatological, hydrological, and meteorological analysis processes in regions with low rain gauge density.

Materials and methods

This section describes the study area, the variables used to develop the convolutional neural network model, data processing, and the procedures applied for its configuration, training, and evaluation.

doi: 10.25100/iyc.v28i1.15228

Location

The Colombian Andean zone is a region highly susceptible to climate variability and faces significant impacts due to the intensity and frequency of extreme events such as droughts and floods. The occurrence of these events is closely related to the warm and cold phases of the El Niño phenomenon, which exhibits teleconnection with local climatic patterns (12,13). The study area corresponds to the zone covered by the Munchique meteorological radar (RMM), located in the municipality of El Tambo (Cauca department), operating within an effective radius of 240 km with measurements every 5 to 10 minutes. It is a C-band PPI (Plan Position Indicator) radar equipped with a dual-polarization receiver/processor, enabling greater precision in distinguishing meteorological and non-meteorological phenomena (Figure. 1).

Within the radar's area of influence, 85 automatic stations provide continuous 10-minute precipitation monitoring, of which 58 are active and free of errors or inconsistencies. According to the World Meteorological Organization (14), in mountainous zones the minimum recommended station density is 250 km² per conventional station and 2,500 km² per automatic station. Regarding the RMM coverage area, the density is on the order of 7,200 km² per automatic station, reflecting very sparse active instrumentation for precipitation monitoring in the region.

Furthermore, the spatial distribution of available stations shows greater concentration in the central zone around the RMM and in the southeast of the influence area, indicating more intensive monitoring in these zones. In contrast, fewer stations are present in the northwest of the departments of Nariño, Cauca, and Valle del Cauca, as well as in southern Chocó and Tolima, highlighting the need to develop and implement methods to merge meteorological information from the pluviometry network and remote sensing products (Figure. 1).

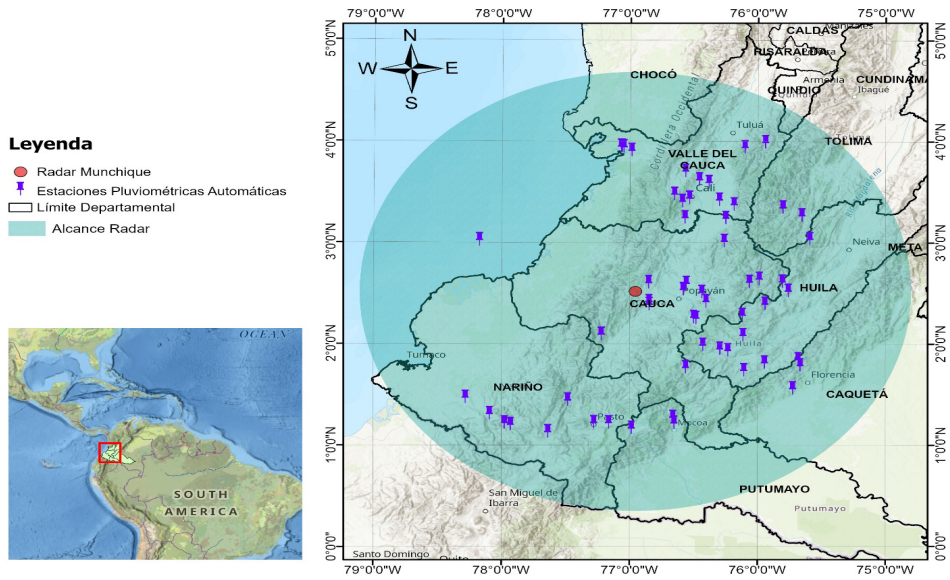

Figure 1. Location of the study area and automatic pluviometry stations used.

doi: 10.25100/iyc.v28i1.15228

Input data

The model input data come from four information sources: satellite images, radar images, automatic rain gauges, and a Digital Elevation Model (DEM) (Table 1). Satellite information is provided by the GOES-16 geostationary environmental operational satellite, which offers broad coverage of almost the entire Western Hemisphere, including North, Central, and South America and parts of the Atlantic and Pacific in full-disk mode. Its Advanced Baseline Imager (ABI) provides high spatial (2 km) and temporal (10 minutes) resolution images. The ABI has 16 spectral channels covering from ultraviolet to infrared, improving the detection and monitoring of cloud formation and evolution, sea surface temperature, and atmospheric humidity. The selected bands as input variables to the model are: Band 7 (3.9 μm) designed to identify fog and low clouds at night, Band 8 (6.19 μm) designed to forecast hurricane tracks and storm motion in mid-latitudes, and Band 13 (10.3 μm) designed to improve atmospheric humidity corrections and cloud identification and classification. The operational characteristics of these infrared (IR) bands are important properties of precipitable clouds (10).

Table 1. Model input variables

Variable	Unit	Description
GOES 16 Band 7	K	Shortwave infrared
GOES 16 Band 8	K	Upper-level water vapor
GOES 16 Band 13	K	Clean infrared window
Reflectivity	dBZ	Radar reflectivity value
Distance to radar	m	Distance to radar
Precipitation	mm/10 min	Station precipitation value
Rain gauge location	Binary	Spatial location of rain gauges
Topography	m	Elevation above sea level
Time of day	Dimensionless	Relative value of the hour

Radar data correspond to equivalent reflectivity (Z), expressed in decibels (dBZ), representing precipitation intensity within the effective radius. This information was provided by the Institute of Hydrology, Meteorology and Environmental Studies of Colombia (IDEAM), the entity responsible for operating and maintaining the instrument. Additionally, distance to the radar was considered as a predictive variable, defined as the distance from each analysis cell to the radar's exact location, aiming to account for possible Earth curvature effects at the limits of the effective range.

Pluviometry information was obtained from IDEAM's hydrometeorological monitoring network, which provides records at monthly, daily, and sub-hourly scales. For this study, records from 58 automatic stations with 10-minute precipitation measurements were used. Since rain gauges provide point data, precipitation for each analysis cell was assigned according to proximity to the nearest rain gauge to the cell center, assigning a null value to cells without available gauges. Additionally, a binary variable indicating rain gauge presence was considered, assigning 0 to cells without stations and 1 otherwise.

doi: 10.25100/iyc.v28i1.15228

Topography plays a fundamental role in the distribution and amount of precipitation, significantly influencing local climatic patterns. This information is provided by the Advanced Land Observing Satellite (ALOS) of the Japan Aerospace Exploration Agency (JAXA), using an L-band synthetic aperture radar sensor (PALSAR) operating at 14 to 28 MHz. A radiometrically terrain-corrected DEM at 90 m spatial resolution was implemented to represent terrain elevation in each cell.

Finally, a dimensionless variable was incorporated to represent the time of day, aiming to analyze systematic variations in infrared radiation data that may occur due to surface temperature changes throughout the day (8). To model time of day as a continuous variable, a cosine transformation was applied, oscillating between 1 at midnight and 0 at noon. Minutes elapsed from midnight are transformed into radians, assigning values proportionally along a full 2π cycle corresponding to an entire day. This methodology is suitable for studies requiring precise examination of diurnal-varying patterns.

The period from February 1 to April 30, 2021, was selected as the analysis window, covering a total of 12,816-time steps represented as input variables to the model. This choice allowed the use of the most relevant and accurate data to evaluate spatiotemporal rainfall dynamics in the case study.

Input layers to the network were provided as multispectral images in TIF format, with an extent of 160 × 160 pixels covering a total area of 102,400 km². All model inputs were spatially rescaled and temporally grouped to the satellite information resolution, i.e., 2 km and 10 minutes, respectively.

Data division

A fundamental strategy for building robust and effective machine learning models is to segment the dataset into three groups: training, validation, and test. This method is crucial to prevent overfitting, ensuring the model achieves an adequate representation of rainfall with unseen data. To achieve this, 70% training, 15% validation, and 15% test split were established.

Considering that rain gauge-observed precipitation is the target variable for modeling, a representative selection of rain gauges was made for subdivision into the three data subsets, based on their spatial and temporal distribution. Spatial selection of rain gauges was performed using stratified random sampling based on the distribution of distances between them. Regarding temporal selection, daily accumulated precipitation was quantified, dates were classified from highest to lowest accumulated precipitation, and they were selected in an ordered and interleaved manner for each subset (training, validation, and test) to ensure homogeneous samples across the three subsets.

Network Architecture

Over the years, convolutional neural network (CNN) architectures have evolved, increasing their accuracy, efficiency, and ability to process images and other spatial data in object recognition, detection, and segmentation tasks (10). Precipitation rate estimation and rainfall probability are classified as segmentation tasks, assigning each image pixel to a binary category (rain/no rain) or

doi: 10.25100/iyc.v28i1.15228

performing regression. In this context, the U-Net architecture, initially proposed by Ronneberger et al. (15) for biomedical image segmentation, has stood out as one of the most effective and widely used due to its ability to work with few data, its symmetric encoder-decoder structure, and skip connections that help preserve important image details.

Therefore, for the present study, a U-Net-type architecture as employed in Moraux et al. (8,9), was implemented, which demonstrated the effectiveness of CNNs for multimodal estimation of precipitation rate and instantaneous rainfall event detection. This architecture outperforms existing techniques and reduces their individual limitations by providing more accurate estimates with better spatial resolution (Figure. 2). The architecture consists of an encoding stage, a decoding stage, and a third stage composed of two subnetworks performing classification and regression tasks.

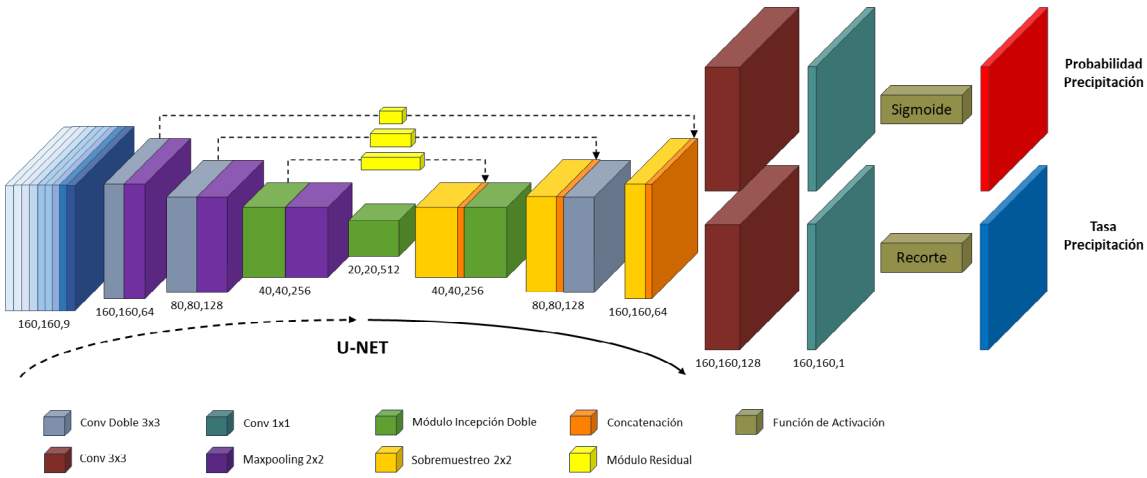

Figure 2. Implemented U-Net architecture

In the encoding stage (contraction), images are downsampled through double convolution layers with 3×3 kernels, followed by batch normalization and ReLU activation. Additionally, image reduction is performed via 2×2 max-pooling layers, allowing the capture of high-level features and abstraction of information. The number of filters in each down-sampling layer is 64, 128, 256, and 512, respectively. Thus, resolution passes from 2 km per pixel (160×160 pixels) at the beginning of encoding to 16 km per pixel (20×20 pixels) at its end. This last constitutes the central core of the network, with the lowest spatial resolution but most complete abstract feature representation.

In the decoding stage (expansion), the network progressively increases image resolution through 2×2 upsampling layers using nearest-neighbor interpolation, followed by 3×3 convolution. This allows reconstruction of the original image but with features learned during encoding. Similarly, double convolution layers have 3×3 kernels, batch normalization, and ReLU activation. The number of filters in each upsampling layer is 512, 256, 128, and 1, respectively, returning the image to the original 2 km per pixel resolution (160×160 pixels) before passing to the two different subnetworks.

As in Moraux et al. (8,9), some convolution layers in encoding and decoding are replaced by double Inception modules proposed by Szegedy et al. (16) in GoogLeNet (Figure. 3These modules

doi: 10.25100/iyc.v28i1.15228

capture more complex features by applying filters of various sizes. Table 2 shows the number of filters configured for each convolution layer implemented in the Inception module. For 5×5 and 7×7 kernels, factorized convolutions are applied following Szegedy et al. (17) enhancing network performance and reducing computational costs.

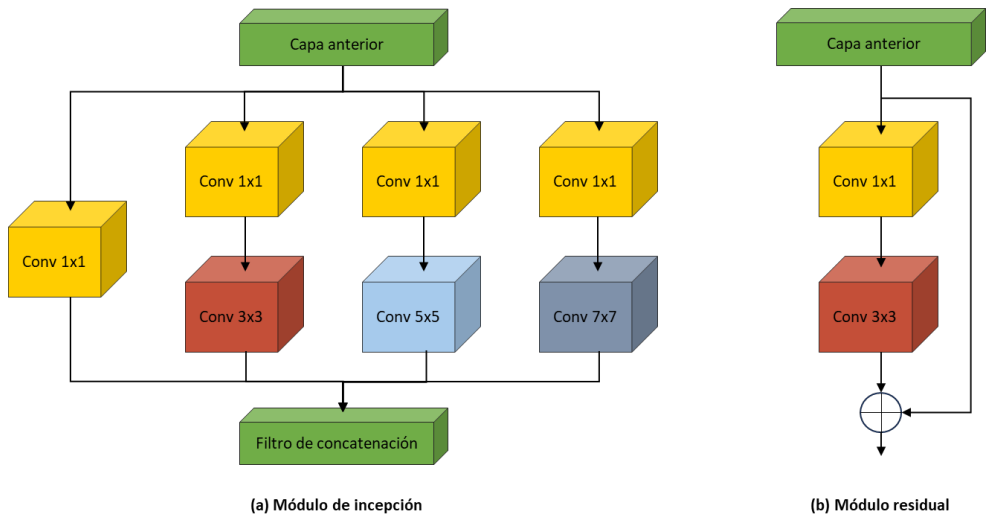

Figure 3. Structure of Inception and residual modules

Table 2. Number of filters in convolutional layers of Inception modules

Output filters	1x1	1x1 (3x3)	3x3	1x1 (5x5)	5x5	1x1 (7x7)	7x7
256	64	128	128	64	32	32	32
512	64	256	384	64	32	32	32

Additionally, skip connections were implemented, directly connecting encoder layers to decoder layers to preserve and recover high-resolution information lost during successive max-pooling layers (Figure. 3). These connections are implemented through residual modules proposed by He et al. (18) as a measure to prevent information degradation in very deep networks, avoiding gradient vanishing and improving accuracy. The union of these layers within the network is performed through feature map concatenation, joining features learned during encoding with upsampling results from decoding.

At the end of the decoder stage, the network branches into two subnetworks responsible for classification and regression tasks, respectively. Each subnetwork consists of a 3×3 convolution layer with batch normalization and ReLU activation, followed by a final 1×1 convolution layer with one output filter. As a result, a feature map of the same dimension as the input image is obtained. The classification head uses a sigmoid activation function, constraining outputs to values between 0 and 1. The regression head uses a clipping function limiting outputs to values between 0 and 100 to bound the maximum simulated precipitation rate.

doi: 10.25100/iyc.v28i1.15228

Training strategy

For the three data subsets (training, validation, and test), at each 10-minute time step, a rain gauge was randomly selected as the target, corresponding to precipitation measured at a specific point/pixel in the Euclidean grid of the study area. Measurements from all other rain gauges, excluding the target gauge at the same time step, were considered as samples and used as input variables to the model. This approach allows evaluation of the network's ability to estimate both precipitation rate and rainfall probability at the target point/pixel, rather than considering multiple targets due to the limited number of available rain gauges. A fundamental aspect in selecting the target rain gauge was ensuring an equitable distribution of zero and positive precipitation values across the three datasets, seeking to balance the amount of data between precipitation and non-precipitation events for balanced training and evaluation.

Since the implemented network is a multitask model estimating rainfall probability and precipitation rate simultaneously, losses are calculated independently with one loss per task. Rainfall probability is a classification task configured with Binary Cross-Entropy (L_{bce}) as the loss function, suitable for problems with instances belonging to one of two possible classes (rain/no rain). Precipitation rate is defined as a regression task configured with Mean Squared Error (L_{mse}), as the loss function, ideal when the prediction responds to continuous values, directly quantifying the magnitude of error between predictions and observed precipitation values. In scenarios where the target precipitation rate is zero (precipitation = 0), the L_{mse} loss is set to 0, so the model only learns from samples with positive precipitation rates (precipitation > 0).

For multitask learning, it is essential to unify losses to balance training and achieve optimal performance across all tasks. The choice of method depends on task nature, data, and specific objectives. For this study, the combined network loss was determined by implementing the Projected Gradient Conflicts (PCGrad) methodology proposed in Yu et al. (19), a powerful strategy in multitask learning leading to substantial gains in efficiency and network performance.

Regarding network optimization, Stochastic Gradient Descent (SGD) with momentum was employed, adjusted using the 1-cycle super-convergence learning rate method proposed by Smith and Topin (20). This method demonstrated that neural networks can be trained faster than with standard training methods, especially useful in scenarios with limited computational resources. The optimal hyperparameter configuration established a batch size of 32, a learning rate of 0.01, and a maximum learning rate of 3×10^{-6}, the latter obtained by implementing the 1-cycle super-convergence learning rate method. The network was trained on an RTX A6000 GPU using the PyTorch library.

Evaluation methods

To evaluate model efficiency in estimating rain/no-rain probability and precipitation rate, seven performance metrics were considered (Table 3). For the classification task, the following indices

doi: 10.25100/iyc.v28i1.15228

were calculated: 1) Probability of Detection (POD), measuring the model's ability to identify positive instances; 2) False Alarm Ratio (FAR), evaluating how often the model incorrectly classifies negative instances as positive; 3) Accuracy (ACC), providing an overall view of model performance by calculating the proportion of correct predictions; 4) F1-score (F1), combining precision and recall; and 5) Receiver Operating Characteristic (ROC) curve, calculated as the area under the curve (AUC), indicating the model's discriminative capacity.

Table 3. Metrics used to evaluate model performance

	Equation	Range	Optimal
Classification scores			
Probability of Detection (POD)	$\mathrm{POD} = \frac{tp}{tp+fn}$	$[0,1]$	1
False Alarm Ratio (FAR)	$\mathrm{FAR} = \frac{fp}{fp+tp}$	$[0,1]$	0
Accuracy (ACC)	$\mathrm{ACC} = \frac{tp+tn}{tp+fp+tn+fn}$	$[0,1]$	1
F1-score (F1)	$\mathrm{F1} = 2 * \frac{P*R}{P+R}, \quad P = \frac{tp}{tp+tn}, \quad R = \frac{tp}{tp+fn}$	$[0,1]$	1
Receiver Operating Characteristic (ROC)	$\mathrm{AUC} = \mathit{Area\ under\ the\ ROC\ curve}$	$[0,1]$	1
tp: true positives; fn: false negatives; fp: false positives; tn: true negatives			
Regression scores			
Mean Absolute Error (MAE)	$\mathrm{MAE} = \frac{1}{N}\sum_{i=1}^{N}\lvert\hat{y}_i - y_i\rvert$	$[0,\infty]$	0
Root Mean Squared Error (RMSE)	$\mathrm{RMSE} = \frac{1}{N}\sum_{i=1}^{N}\sqrt{(\hat{y}_i - y_i)^2}$	$[0,\infty]$	0
y_i: observed value, $\hat{y}$: estimated value			

Table 4 details the contingency values between observations and estimates required for calculating classification-related metrics. For the regression task, Mean Absolute Error (MAE) was calculated, interpreting the average magnitude of model errors without considering direction; and Root Mean Squared Error (RMSE), indicating on average how far model predictions are from actual values.

Another relevant aspect was the categorization of rainy and non-rainy days from the probability values generated by the trained network. For this, it was necessary to establish the probability threshold defining class separation, optimized as a hyperparameter by maximizing the area under the ROC curve (AUC) on the aggregated training and validation datasets.

doi: 10.25100/iyc.v28i1.15228

Table 4. Classification contingency table

		Observed	
		$r = 0$	$r > 0$
Estimated	$r = 0$	tn	fn
	$r > 0$	fp	tp

tn: true negatives, fn: false negatives,
fp: false positives, tp: true positives

Results and discussion

During the training phase, the implemented convolutional neural network (CNN) showed successful convergence after 17 epochs, identified as the optimal balance point between underfitting and overfitting, i.e., the best fit point of the network (Figure. 4). n all three data subsets, losses decreased consistently as the model progressed through epochs, evidencing effective learning. Training and validation sets exhibited similar behavior, characterized by loss reduction and stabilization. Although the test set showed some variability, it also evidenced a decrease in losses, suggesting the model's potential to generalize to unseen data.

On the other hand, in the classification task, the model demonstrates significant improvement in identifying rain and no-rain events. Area Under the Curve (AUC) values are 0.80 for training, 0.79 for validation, and 0.80 for test, considered acceptable and indicating good discriminative capacity. Analyzing metrics associated with the network's classification capability, a high Probability of Detection (POD) index of 0.80 is observed in the validation set, evidencing the model's efficacy in detecting rainfall events. The False Alarm Ratio (FAR) presents average values of 0.21 across the three datasets, indicating a moderate tendency to correctly classify no-rain events. Accuracy (ACC) and F1 metrics show the model maintains consistent precision (around 0.62 in validation), highlighting its solid performance in the classification task.

Regarding the network's regression task, when comparing observed versus simulated precipitation rate, the model shows inability to adequately capture extreme precipitation values, tending to underestimate intense events. Additionally, data scatter is observed, suggesting the model does not optimally perform its regression function. Analyzing the metrics calculated to evaluate model efficiency, RMSE values of 1.04, 1.02, and 1.07 mm were obtained in training, validation, and test, respectively. Mean Absolute Error (MAE) is 0.44, 0.48, and 0.51 for the three subsets, respectively, but the coefficient of determination (R^2) evidence that the regression task reaches only 0.29, 0.36, and 0.05% explained variance. These results indicate the model adequately captures rainfall occurrence probability but does not achieve acceptable performance in predicting rainfall amounts in millimeters.

doi: 10.25100/iyc.v28i1.15228

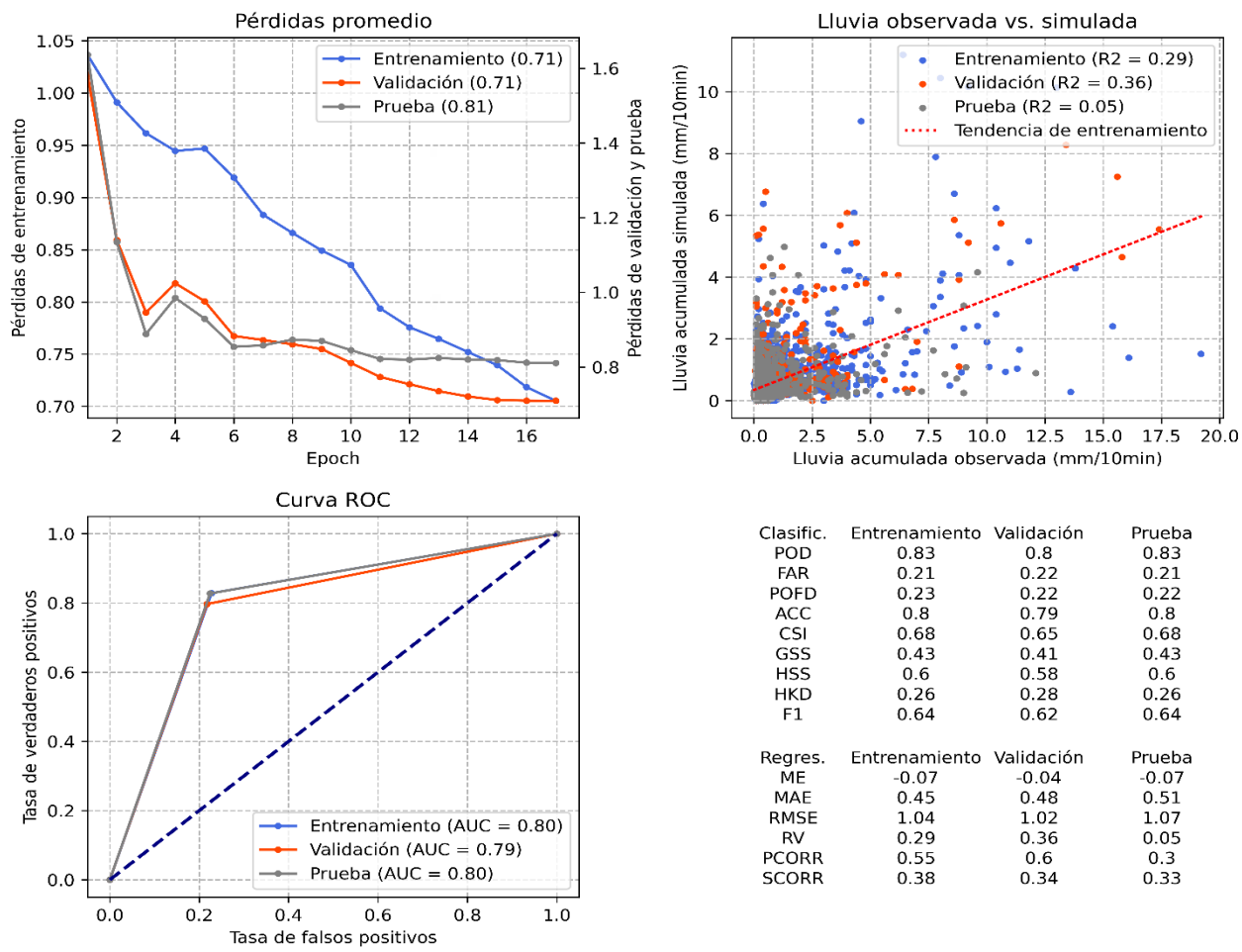

Clasific.	Entrenamiento	Validación	Prueba
POD	0.83	0.8	0.83
FAR	0.21	0.22	0.21
POFD	0.23	0.22	0.22
ACC	0.8	0.79	0.8
CSI	0.68	0.65	0.68
GSS	0.43	0.41	0.43
HSS	0.6	0.58	0.6
HKD	0.26	0.28	0.26
F1	0.64	0.62	0.64

Regres.	Entrenamiento	Validación	Prueba
ME	-0.07	-0.04	-0.07
MAE	0.45	0.48	0.51
RMSE	1.04	1.02	1.07
RV	0.29	0.36	0.05
PCORR	0.55	0.6	0.3
SCORR	0.38	0.34	0.33

Figure 4. Losses of the training, validation, and test sets during model training

When evaluating network behavior across training epochs, Table 5 shows continuous improvement in most metrics until epoch 17, indicating the model efficiently learns and fits rainfall occurrence probability data. These improvements correspond to a notable increase in rain detection (POD) and reduction in false alarms (FAR), especially in training and validation. Satisfactory performance was also achieved in metrics such as accuracy (ACC) and area under the curve (ROC), even in the test phase. For the regression task, marginal reduction is observed in MAE and RMSE indices, demonstrating that the convolutional neural network structure would require coupling with time-series models to more efficiently learn the temporal dependency structure of the data.

In line with our findings, other authors have identified limitations in convolutional neural networks (CNNs) for reproducing temporal correlations in time series, affecting accuracy in regression tasks. Han et al. (21) observed that, in the context of subsurface ocean temperature estimation in the Pacific, CNNs do not adequately capture temporal correlation of series, underestimating extreme variations and showing dispersion like that detected in precipitation rate quantification in this study. Similarly, Badrinath et al. (22) reported improvements in daily accumulated precipitation prediction using CNNs; however, they highlight that long temporal dependencies are not efficiently

doi: 10.25100/iyc.v28i1.15228

modeled, suggesting integration of recurrent neural networks could mitigate these issues. In this context, studies such as Shi et al. (23) have shown promising results in simultaneously predicting both tasks (rainfall probability and rainfall amount) by applying a double machine learning approach combined with recurrent neural networks and convolutional structures, achieving satisfactory correlation coefficients in validation. These results highlight the need for hybrid architecture in the convolutional network model developed in this research to reduce underestimation of intense events.

Table 5. Evolution of model efficiencies

	Training		Validation		Test	
	Ep1	Ep17	Ep1		Ep1	
POD	0.79	0.85	0.66	0.80	0.69	0.83
FAR	0.39	0.21	0.31	0.22	0.35	0.21
ACC	0.64	0.81	0.68	0.79	0.66	0.80
F1	0.69	0.65	0.56	0.62	0.60	0.64
ROC	0.64	0.81	0.68	0.79	0.66	0.80
MAE	0.54	0.44	0.58	0.48	0.58	0.51
RMSE	1.23	1.01	1.35	1.02	1.22	1.07

Conclusions

The convolutional neural network (CNN) implemented in this study has demonstrated significant performance in detecting rainfall occurrence probability in a low-instrumentation region. The model showed satisfactory performance in detecting rain and no-rain patterns, reflected in the obtained efficiencies and metrics such as Area Under the Curve (AUC) and Probability of Detection (POD) index.

Despite positive results in rainfall event classification, the need to improve quantitative precipitation rate estimation was identified. RMSE and MAE values suggest the model still does not fully capture relationships between observed and simulated precipitation rates. This highlights the importance of strengthening the monitoring network to achieve greater spatial representativeness, which would contribute to better representation of rainfall magnitude.

Acknowledgements
The authors thank Universidad del Tolima for financial support for the research execution through project 80623 of 2023 (agreement 601-2023).

Funding
Universidad del Tolima project 80623 of 2023 (agreement 601-2023).

CrediT authorship contribution statement
Conceptualization - Ideas: Henry Rubiano, Miguel Barrios. Data curation: Henry Rubiano. Formal analysis: Cristian Guevara, Henry Rubiano, Miguel Barrios. Investigation: Henry Rubiano. Methodology: Cristian Guevara, Henry Rubiano, Miguel Barrios. Project Management: Miguel Barrios. Resources: Miguel Barrios. Software: Miguel Barrios. Supervision: Miguel Barrios. Validation:

doi: 10.25100/iyc.v28i1.15228

Cristian Guevara, Miguel Barrios. Writing - original draft - Preparation: Henry Rubiano, Cristian Guevara, Miguel Barrios. Writing - revision and editing -Preparation: Cristian Guevara, Miguel Barrios

References

1. Valencia S, Marín DE, Gómez D, Hoyos N, Salazar JF, Villegas JC. Spatio-temporal assessment of Gridded precipitation products across topographic and climatic gradients in Colombia. Atmos Res [Internet]. 2023;285:106643.

https://doi.org/10.1016/j.atmosres.2023.106643

2. Hou AY, Kakar RK, Neeck S, Azarbarzin AA, Kummerow CD, Kojima M, et al. The Global Precipitation Measurement Mission. Bull Am Meteorol Soc [Internet]. 2014;95(5):701-22.

https://doi.org/10.1175/BAMS-D-13-00164.1

3. Baez-Villanueva OM, Zambrano-Bigiarini M, Ribbe L, Nauditt A, Giraldo-Osorio JD, Thinh NX. Temporal and spatial evaluation of satellite rainfall estimates over different regions in Latin-America. Atmos Res [Internet]. 2018;213:34-50.

https://doi.org/10.1016/j.atmosres.2018.05.011

4. Baez-Villanueva OM, Zambrano-Bigiarini M, Beck HE, McNamara I, Ribbe L, Nauditt A, et al. RF-MEP: A novel Random Forest method for merging gridded precipitation products and ground-based measurements. Remote Sens Environ [Internet]. 2020;239:111606.

https://doi.org/10.1016/j.rse.2019.111606

5. Chen S, Xiong L, Ma Q, Kim JS, Chen J, Xu CY. Improving daily spatial precipitation estimates by merging gauge observation with multiple satellite-based precipitation products based on the geographically weighted ridge regression method. J Hydrol (Amst) [Internet]. 2020;589:125156.

https://doi.org/10.1016/j.jhydrol.2020.125156

6. Zhang L, Li X, Zheng D, Zhang K, Ma Q, Zhao Y, et al. Merging multiple satellite-based precipitation products and gauge observations using a novel double machine learning approach. J Hydrol (Amst) [Internet]. 2021;594:125969.

https://doi.org/10.1016/j.jhydrol.2021.125969

7. Han Y, Wu J, Zhai B, Pan Y, Huang G, Wu L, et al. Coupling a Bat Algorithm with XGBoost to Estimate Reference Evapotranspiration in the Arid and Semiarid Regions of China. Advances in Meteorology [Internet]. 2019;2019(1):9575782.

https://doi.org/10.1155/2019/9575782

8. Moraux A, Dewitte S, Cornelis B, Munteanu A. Deep Learning for Precipitation Estimation from Satellite and Rain Gauges Measurements. Remote Sens (Basel) [Internet]. 2019;11(21).

https://doi.org/10.3390/rs11212463

9. Moraux A, Dewitte S, Cornelis B, Munteanu A. A Deep Learning Multimodal Method for Precipitation Estimation. Remote Sens (Basel) [Internet]. 2021;13(16).

https://doi.org/10.3390/rs13163278

10. Wang C, Tang G, Xiong W, Ma Z, Zhu S. Infrared precipitation estimation using convolutional neural network for FengYun satellites. J Hydrol (Amst) [Internet]. 2021;603:127113.

https://doi.org/10.1016/j.jhydrol.2021.127113

doi: 10.25100/iyc.v28i1.15228

11. Wang C, Xu J, Tang G, Yang Y, Hong Y. Infrared Precipitation Estimation Using Convolutional Neural Network. IEEE Transactions on Geoscience and Remote Sensing. diciembre de 2020;58(12):8612-25.

https://doi.org/10.1109/TGRS.2020.2989183

12. Poveda G, Álvarez D, Rueda Ó. Hydro-climatic variability over the Andes of Colombia associated with ENSO: a review of climatic processes and their impact on one of the Earth's most important biodiversity hotspots. Clim Dyn [Internet]. 2011;36:2233-49.

https://doi.org/10.1007/s00382-010-0931-y

13. Salas HD, Builes-Jaramillo A, Boers N, Poveda G, Mesa ÓJ, Kurths J. Precipitation over northern South America and the far-eastern Pacific during ENSO: Phase synchronization at inter-annual time scales. International Journal of Climatology [Internet]. 2024;44(6):2106-23.

https://doi.org/10.1002/joc.8443

14. World Meteorological Organization. Guide to Hydrological Practice. Volume I: Hydrology from Measurement to Hydrological Information. WMO-No. 168 [Internet]. Vol. Volume 1. Geneva: World Meteorological Organization; 2025 [citado el 7 de septiembre de 2025]. Disponible en: https://library.wmo.int/idurl/4/35804

15. Ronneberger Olaf, Fischer P, Brox Thomas. U-Net: Convolutional Networks for Biomedical Image Segmentation. En: Navab Nassir and Hornegger J and WWM and FAF, editor. Medical Image Computing and Computer-Assisted Intervention - MICCAI 2015. Cham: Springer International Publishing; 2015. p. 234-41.

https://doi.org/10.1007/978-3-319-24574-4_28

16. Szegedy C, Liu W, Jia Y, Sermanet P, Reed S, Anguelov D, et al. Going deeper with convolutions. En: 2015 IEEE Conference on Computer Vision and Pattern Recognition (CVPR). 2015. p. 1-9.

https://doi.org/10.1109/CVPR.2015.7298594

17. Szegedy C, Vanhoucke V, Ioffe S, Shlens J, Wojna Z. Rethinking the Inception Architecture for Computer Vision. En: 2016 IEEE Conference on Computer Vision and Pattern Recognition (CVPR). 2016. p. 2818-26.

https://doi.org/10.1109/CVPR.2016.308

18. He K, Zhang X, Ren S, Sun J. Deep Residual Learning for Image Recognition. En: Proceedings of the IEEE Conference on Computer Vision and Pattern Recognition (CVPR). 2016.

https://doi.org/10.1109/CVPR.2016.90

19. Yu T, Kumar S, Gupta A, Levine S, Hausman K, Finn C. Gradient Surgery for Multi-Task Learning. En: Larochelle H, Ranzato M, Hadsell R, Balcan MF, Lin H, editores. Advances in Neural Information Processing Systems [Internet]. Curran Associates, Inc.; 2020. p. 5824-36. Disponible en: https://proceedings.neurips.cc/paper_files/paper/2020/file/3fe78a8acf5fda99de95303940a2420c-Paper.pdf

20. Smith LN, Topin N. Super-convergence: very fast training of neural networks using large learning rates. En: Pham T, editor. Artificial Intelligence and Machine Learning for Multi-Domain Operations Applications [Internet]. SPIE; 2019. p. 1100612.

https://doi.org/10.1117/12.2520589

21. Han M, Feng Y, Zhao X, Sun C, Hong F, Liu C. A Convolutional Neural Network Using Surface Data to Predict Subsurface Temperatures in the Pacific Ocean. IEEE Access. septiembre de 2019;7:172816-29.

https://doi.org/10.1109/ACCESS.2019.2955957

22. Badrinath A, Monache LD, Hayatbini N, Chapman W, Cannon F, Ralph M. Improving Precipitation Forecasts with Convolutional Neural Networks. Weather Forecast [Internet]. 2023;38(2):291-306. Disponible en: https://journals.ametsoc.org/view/journals/wefo/38/2/WAF-D-22-0002.1.xml

23. Shi X, Chen Z, Wang H, Yeung DY, Wong W kin, Woo W chun. Convolutional LSTM Network: A Machine Learning Approach for Precipitation Nowcasting. En: Cortes C, Lawrence N, Lee D, Sugiyama M, Garnett R, editores. Advances in Neural Information Processing Systems [Internet]. Curran Associates, Inc.; 2015. Disponible en: https://proceedings.neurips.cc/paper_files/paper/2015/file/07563a3fe3bbe7e3ba84431ad9d055af-Paper.pdf

doi: 10.25100/iyc.v28i1.15228